Compact Filtering Balun With Wide Stopband and Low Radiation Loss Using Hybrid Microstrip and Substrate-Integrated Defected Ground Structure

Deshan Tang, *Student Member, IEEE* and Xun Luo, *Senior Member, IEEE*

***Abstract*— In this letter, a novel hybrid microstrip and substrate-integrated defected ground structure (SIDGS) are proposed for filtering balun design. Coupled microstrip and SIDGS resonators can not only achieve 180° phase imbalance with filtering response but also realize wide stopband and wideband low radiation loss. In addition, the feature of stacked substrate packaging could reduce the size of the circuit and be flexible for integration. To verify this mechanism, a filtering balun operating at 3.08 GHz with 3-dB fractional bandwidth (FBW) of 45% is proposed based on hybrid microstrip and SIDGS, which exhibits the in-band amplitude- and phase-imbalances of ±0.5 dB and ±0.4°, respectively. The stopband extends to 18 GHz with the rejection level of 20 dB, whereas the measured total loss (i.e., including radiation, metal, and substrate loss) is less than 15% up to 15.3 GHz.**

***Index Terms*— Filtering balun, low radiation loss, microstrip, substrate-integrated defected ground structure (SIDGS), wide stopband.**

I. Introduction

With the ever-increasing development of wireless systems, wideband interference suppression becomes a major challenge for the design of passive components. As a crucial component in wireless systems, the balun [1]–[9] has drawn great attention recently. In [10] and [11], the substrate integrated waveguide (SIW) is applied to balun design with good in-band performance and low radiation loss, while it is limited by the narrow stopband and large size. To extend the stopband bandwidth of balun, the stepped impedance resonators [12], stepped coupled lines [13], and high-order planar structure [14] are proposed. However, these baluns could easily generate high radiation at stopband. Recently, substrate-integrated defected ground structure (SIDGS) [15], [16] is developed with wide stopband and wideband low radiation loss. Nevertheless, the design of filtering balun with good in-band performance, wide stopband, and wideband low radiation loss, and compact size for flexible integration remains a great challenge.

In this letter, a hybrid microstrip and SIDGS are proposed and utilized for the compact filtering balun design with high performance. Two identical SIDGS resonators and a stepped-impedance microstrip resonator are used in such balun. With a proper coupling scheme, the function of filtering balun (i.e., 180° phase imbalance in the passband) can be achieved. The harmonic suppression characteristic of two kinds of resonators could introduce a wide stopband response. At the same time, the microstrip is integrated with SIDGS. Such implementation can not only minimize the radiation loss in a wide frequency range but also miniaturize the circuit size.

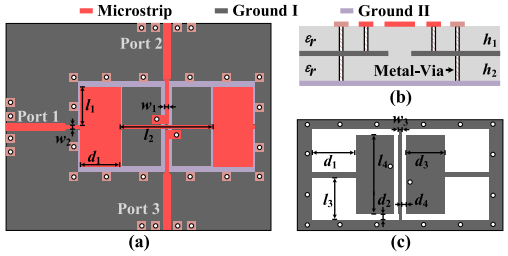

Fig. 1. Configuration of the proposed hybrid microstrip and SIDGS balun. (a) Top view. (b) Layer diagram. (c) Details of ground I.

II. Schematic and Operation

Fig. 1 depicts the configuration of the hybrid microstrip and SIDGS balun. The balun is composed of two SIDGS resonators and a microstrip resonator, which are integrated at different layers with the surrounding ground and metal-vias. Here, the physical size of these DGSs cannot meet the theoretical definition of slotline [17, p. 246]. To further investigate the mechanism of the proposed balun, the dielectric substrate RO4003C (i.e., $\varepsilon_r = 3.55$, $h_1 = 0.203$ mm, and $h_2 = 0.303$ mm) and electromagnetic (EM)-simulator HFSS are used.

A. Microstrip Resonator and SIDGS Resonator

1) Microstrip Resonator: Fig. 2(a) and (b) depicts the configuration and equivalent circuit of the microstrip resonator. Then, the input admittance of the resonator (i.e., Y_A) can be derived by (1), as shown at the bottom of the next page. The fundamental resonant frequency (i.e., f_{A0}) of the resonator is obtained when $Y_A = 0$. Fig. 2(c) provides the calculated and simulated fundamental resonant frequency f_{A0} versus l_1 and w_2, respectively. Here, the electrical length and characteristic impedance of the microstrip could be calculated [18, p. 148]. To investigate the harmonic characteristics of the microstrip resonator, the simulated transmission response of

Manuscript received February 11, 2021; revised March 8, 2021; accepted March 9, 2021. Date of publication March 10, 2021; date of current version June 7, 2021. This work was supported by the NSFC under Grant 61934001. *(Corresponding author: Xun Luo.)*

The authors are with the Center for Advanced Semiconductor and Integrated Micro-System, University of Electronic Science and Technology of China, Chengdu 611731, China (e-mail: xun-luo@ieee.org).

Color versions of one or more figures in this letter are available at https://doi.org/10.1109/LMWC.2021.3065416.

Digital Object Identifier 10.1109/LMWC.2021.3065416

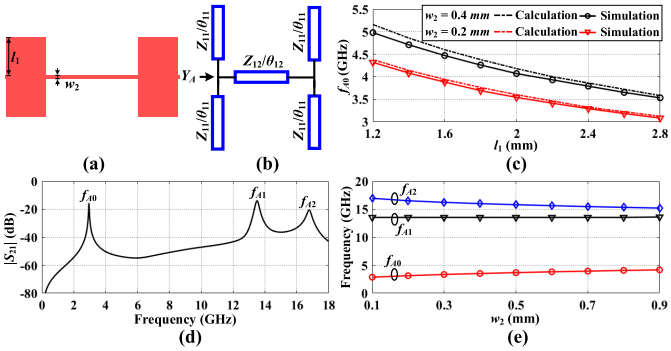

Fig. 2. (a) Configuration of the microstrip resonator. (b) Simplified equivalent circuit model. (c) Effect of l_1 and w_2 on the resonant frequency of the microstrip resonator. (d) Simulated frequency response of week-coupled microstrip resonator. (e) Effect of w_2 on the fundamental and spurious resonant frequencies.

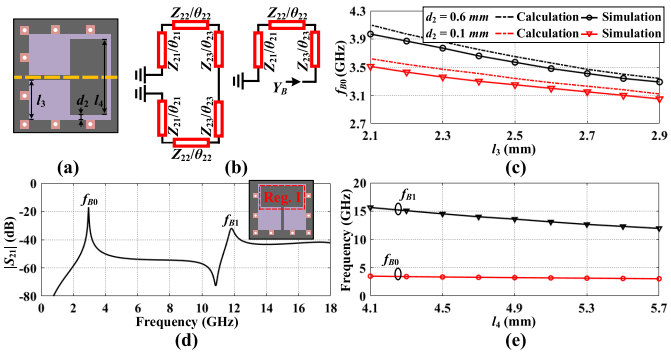

Fig. 3. (a) Configuration of the SIDGS resonator. (b) Simplified equivalent circuit model. (c) Effect of l_3 and d_2 on the resonant frequency of the SIDGS resonator. (d) Simulated frequency response of week-coupled SIDGS resonator. (e) Effect of l_4 on the fundamental and spurious resonant frequencies.

the weak-coupled feeding scheme is presented in Fig. 2(d). It is known that the resonator using stepped-impedance can shift the harmonic to higher frequency [19]. To illustrate the relationship between the harmonic and impedance Z_{12} of the microstrip resonator, Fig. 2(e) depicts the fundamental, first and second harmonic resonant frequencies versus w_2. With the decreasing of the impedance Z_{12} (i.e., the increase of w_2), the fundamental resonant frequency increases while the second harmonic resonant frequency decreases.

2) SIDGS Resonator: Fig. 3(a) and (b) depicts the configuration and equivalent circuit of the SIDGS resonator. The proposed structure is symmetric to the dotted line. Then, the even-mode input admittance of the resonator (i.e., Y_B) is derived by (2), as shown at the bottom of the page. The fundamental resonant frequency (i.e., f_{B0}) of the resonator is obtained under the case of $Y_B = 0$. Fig. 3(c) provides the calculated and simulated fundamental resonant frequency f_{B0} with the variation of d_2 and l_3, respectively. The electrical length and characteristic impedance of the SIDGS can be extracted by simulation. To verify the harmonic characteristic

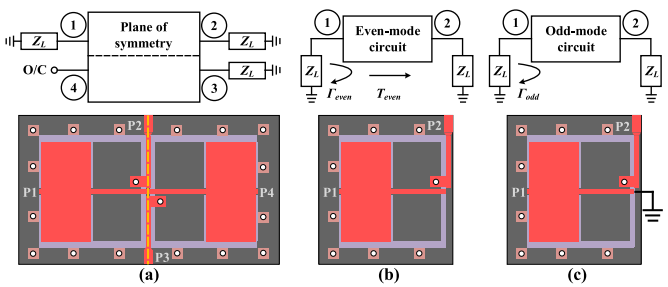

Fig. 4. (a) Balun configured as a symmetrical four-port network with one port terminated in open circuit. (b) Even-mode circuit. (c) Odd-mode circuit.

of the SIDGS resonator, the simulated transmission responses in the weak-coupled feeding scheme are presented in Fig. 3(d). Note that the first harmonic of this SIDGS resonator is mainly caused by the TEM spurious resonant mode due to the rectangular metal patch in Reg. I. To illustrate the relationship between the harmonic and the length of rectangular metal patch, Fig. 3(e) depicts the fundamental and first harmonic resonant frequency versus l_4. With the decreasing length of the metal pad, the first harmonic resonant frequency increases sharply while the fundamental resonant frequency increases slightly.

B. Filtering Balun Design

1) Analysis of Phase Characteristic: The balun could be described as a symmetrical four-port network, where port 4 is terminated with an open circuit, as shown in Fig. 4(a). Fig. 4(b) and (c) illustrates the even- and odd-mode equivalent circuits, respectively. To satisfy the 180° phase difference between port 2 and port 3, the following condition is required [20]:

$$\frac{T_{\text{even}}(1-\Gamma_{\text{odd}})}{2-\Gamma_{\text{even}}-\Gamma_{\text{odd}}}=0. \tag{3}$$

Γ_{even} and Γ_{odd} are the input reflection coefficients of the even- and odd-mode circuits, respectively, and T_{even} denotes the transmission coefficient of the even-mode circuit. In the even-mode circuit, the fundamental resonant frequency of the SIDGS resonator is 3 GHz while the fundamental resonant frequency of the microstrip resonator is 13.3 GHz. Note that the operating frequency of the balun is designed at 3 GHz. When the even-mode circuit operated at 3 GHz, the microstrip resonator is far below the resonant frequency, which can hardly store energy. Therefore, the coupling coefficient between two resonators in an even-mode circuit could approximately equal to zero. Thus, the even-mode circuit features a transmission stop and $T_{\text{even}} = 0$, which satisfies (3).

2) Analysis of Filtering Response: To determine the passband frequency response of the balun, the configuration of the three-port coupling scheme is depicted in Fig. 5. Since the circuit is symmetrical, a two-port second-order topology

$$Y_A = \frac{j}{Z_{12}}\frac{2Z_{12}\tan\theta_{11}+Z_{11}\tan\theta_{12}}{Z_{11}-2Z_{12}\tan\theta_{11}\tan\theta_{12}}+\frac{2j\tan\theta_{11}}{Z_{11}} \tag{1}$$

$$Y_B = -j\frac{1}{Z_{23}}\frac{Z_{22}Z_{23}-Z_{21}Z_{23}\tan\theta_{21}\tan\theta_{22}-Z_{21}Z_{22}\tan\theta_{21}\tan\theta_{23}-Z_{22}^2\tan\theta_{22}\tan\theta_{23}}{Z_{21}Z_{22}\tan\theta_{21}+Z_{22}^2\tan\theta_{22}+Z_{22}Z_{23}\tan\theta_{23}-Z_{21}Z_{23}\tan\theta_{21}\tan\theta_{22}\tan\theta_{23}}. \tag{2}$$

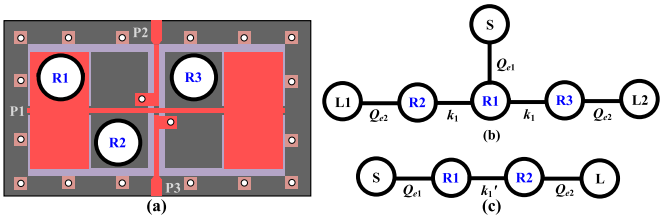

Fig. 5. (a) Configuration of three coupled resonators. (b) Three-port coupling scheme. (c) Simplified two-port coupling scheme with same source impedance.

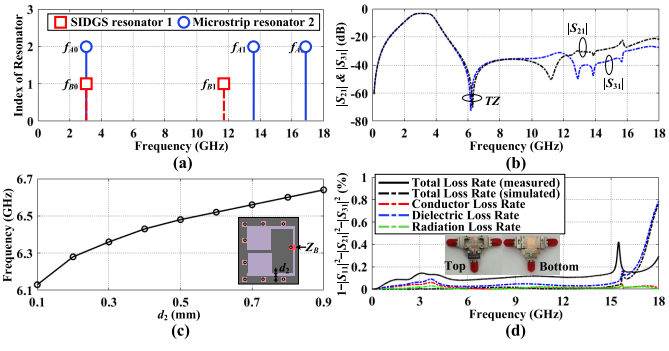

Fig. 6. (a) Comparison of the fundamental and harmonic resonant frequencies of microstrip and SIDGS resonators. (b) Simulated transmission responses of the proposed balun. (c) Effect of d_2 on the frequency of the transmission zero. (d) Simulated and measured loss responses with the photograph of the balun ($l_1 = 2.79$, $l_2 = 5$, $l_3 = 2.78$, $l_4 = 5.73$, $d_1 = 2.85$, $d_2 = 0.1$, $d_3 = 2.2$, $d_4 = 0.19$, $w_1 = 0.28$, $w_2 = 0.16$ and $w_3 = 0.1$, unit: mm).

is used for simplifying the analysis of the circuit. In order to remain the same source impedance of two circuits, k_1 should equal to $k_1'/\sqrt{2}$ [21]. To calculate all the coupling coefficients of the balun, the coupling coefficients of the two-port circuit should be firstly determined according to the filtering specification (i.e., centered at 3 GHz with 3-dB bandwidth of 45%). The specification could be satisfied when $m_1' = 0.884$, $m_{S1} = 0.914$, and $m_{2L} = 0.9$. By using the formulas in [22], $k_1' = 0.398$, $Q_{e1} = 2.66$, $Q_{e2} = 2.74$, and k_1 could be calculated as 0.281. Therefore, the passband response of the balun could be achieved, when the coupling coefficients extracted from the balun are consistent with the calculated results [22].

To discuss the harmonic suppression of the balun, the fundamental and harmonic resonant frequencies of microstrip and SIDGS resonators are presented in Fig. 6(a). Note that the high-order harmonics of these two kinds of resonators are separated. Thus, these resonators serve as the spurious-blocking resonators to suppress the spurious passbands [23]. Moreover, Fig. 6(b) depicts a transmission zero located at the upper side of the passband, which enhances the stopband rejection level. The center-tapped SIDGS resonator could be regarded as a short stub, which can generate a transmission zero under the case of $Z_B = 0$ [24]. Fig. 6(c) provides the simulated transmission zero frequency versus d_2.

3) Radiation Loss: The EM-field of DGS is divergent in an open space, leading to large radiation. Such radiation could cause an extra insertion loss and EM interference to adjacent devices. SIDGS is proposed to confine most of the divergent EM-field, which effectively reduces the radiation loss compared to the conventional DGS [15], [16]. In this balun design, the microstrip is integrated with the SIDGS by the surrounding ground and metal-vias. Radiation/conductor/dielectric loss rates of the balun are shown in Fig. 6(d). The radiation loss is less than 10% (i.e., <0.46 dB) up to 15.7 GHz.

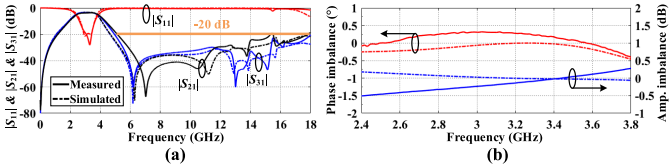

Fig. 7. Measured and simulated results of the proposed balun. (a) *S*-parameters. (b) In-band amplitude- and phase-imbalances.

TABLE I
COMPARISON OF STATE-OF-THE-ARTS FILTERING BALUN

Ref.	[11]	[12]	[14]	**This Work**
Technology	SIW	Microstrip	Microstrip	**SIDGS**
f_0(GHz)	10.46	2	1	**3.08**
IL*(dB)	1.4	0.9	1.07	**0.6**
FBW(%)	6	5	112	**45**
A.-Im(dB)/ P.-Im(°)**	1.5/3	0.3/3.5	0.4/2	**0.5/0.4**
Stopband Rejection	N/A	>25 dB up to $3.5f_0$	>23 dB up to $5.2f_0$	**>20 dB up to $5.8f_0$**
Radiation Loss$^{\Delta}$	Low	medium	High	**<10% (Low) up to $5.1f_0$**
Total Loss <15%$^{\diamond}$	Up to $1.2f_0$$^{\diamond\diamond}$	Up to $3.5f_0$$^{\diamond\diamond}$	Up to $2f_0$$^{\diamond\diamond}$	**Up to $5f_0$**
Core Size	2295 mm^2	2264 mm^2	2150 mm^2	**0.024 (λ_g^2) 91.7 mm^2**

*: Insertion loss. **: Amplitude-Imbalance/Phase-Imbalance.
$^{\Delta}$: Calculated radiation loss under case of lossless substrate and metal.
$^{\diamond}$: Measured total loss including radiation, metal, and substrate loss.
$^{\diamond\diamond}$: Estimated from the paper.

III. FABRICATION AND MEASUREMENT

Based on the structures mentioned above, a compact filtering balun is fabricated, as shown in Fig. 6(d). The simulated and measured results of *S*-parameters are depicted in Fig. 7. The Agilent 5230A network analyzer is used to measure. The center frequency of the balun is 3.08 GHz with a 3-dB fractional bandwidth (FBW) of 45%. The minimum in-band insertion loss is 0.6 dB excluding the theoretical 3-dB loss. The in-band amplitude- and phase-imbalances are ±0.5 dB and ±0.4°, respectively. At the same time, the stopband is up to 18 GHz with a rejection level higher than 20 dB. The total loss is less than 15% (i.e., <0.7 dB) up to 15.3 GHz, as shown in Fig. 6(d). The core size is about 0.12 $\lambda_g \times 0.2\ \lambda_g$, where λ_g is the microstrip guided wavelength at the center frequency. A comparison of the filtering balun with the state-of-the-arts is shown in Table I, The proposed balun has merits of good in-band performance, wide stopband, wideband low radiation loss, and compact size.

IV. CONCLUSION

In this letter, a novel hybrid microstrip and SIDGS is proposed for filtering balun design, which can not only achieve 180° phase difference in a compact size but also inherit the merits of SIDGS such as wide stopband and low radiation loss. Based on such structure, a filtering balun is developed with low insertion loss, low in-band amplitude- and phase-imbalances, wideband harmonic suppression, and wideband low radiation loss. With such good performances, such balun is attractive for integrated systems with wideband spurious suppression and low radiation.

REFERENCES

[1] K. S. Ang and I. D. Robertson, "Analysis and design of impedance-transforming planar Marchand baluns," *IEEE Trans. Microw. Theory Techn.*, vol. 49, no. 2, pp. 402–406, Feb. 2001.

[2] F. Zhu, W. Hong, J.-X. Chen, and K. Wu, "Ultra-wideband single and dual baluns based on substrate integrated coaxial line technology," *IEEE Trans. Microw. Theory Techn.*, vol. 60, no. 10, pp. 3062–3070, Oct. 2012.

[3] I. Piekarz, J. Sorocki, S. Gruszczynski, and K. Wincza, "Input match and output balance improvement of Marchand balun with connecting line," *IEEE Microw. Wireless Compon. Lett.*, vol. 24, no. 10, pp. 683–685, Oct. 2014.

[4] J. H. Lee, J. A. Park, C. S. Cho, and J. W. Lee, "New design formulas for asymmetric coupled-section Marchand balun," *IEEE Microw. Wireless Compon. Lett.*, vol. 25, no. 7, pp. 448–450, Jul. 2015.

[5] T. Canning, J. R. Powell, and S. C. Cripps, "Optimal design of broadband microwave baluns using single-layer planar circuit technology," *IEEE Trans. Microw. Theory Techn.*, vol. 62, no. 5, pp. 1183–1191, May 2014.

[6] M. Frank, M. Thorsell, and P. Enoksson, "Design equations for lumped element balun with inherent complex impedance transformation," *IEEE Trans. Microw. Theory Techn.*, vol. 65, no. 12, pp. 5162–5170, Dec. 2017.

[7] T. Zhang, L. Li, Z. Zhu, and T. J. Cui, "A broadband planar balun using aperture-coupled microstrip-to-SIW transition," *IEEE Microw. Wireless Compon. Lett.*, vol. 29, no. 8, pp. 532–534, Aug. 2019.

[8] A. K. Gorur, "A dual-band balun BPF using codirectional split ring resonators," *IEEE Microw. Wireless Compon. Lett.*, vol. 30, no. 10, pp. 949–952, Oct. 2020.

[9] M. H. Maktoomi, H. Ren, M. N. Marbell, V. Klein, R. Wilson, and B. Arigong, "A wideband isolated real-to-complex impedance transforming uniplanar microstrip line balun for push–pull power amplifier," *IEEE Trans. Microw. Theory Techn.*, vol. 68, no. 11, pp. 4560–4569, Nov. 2020.

[10] Z.-Y. Zhang and K. Wu, "A broadband substrate integrated waveguide (SIW) planar balun," *IEEE Microw. Wireless Compon. Lett.*, vol. 17, no. 12, pp. 843–845, Dec. 2007.

[11] L.-S. Wu, Y.-X. Guo, J.-F. Mao, and W.-Y. Yin, "Design of a substrate integrated waveguide balun filter based on three-port coupled-resonator circuit model," *IEEE Microw. Wireless Compon. Lett.*, vol. 21, no. 5, pp. 252–254, May 2011.

[12] P. Kim, W. Qi, G. Chaudhary, and Y. Jeong, "A design of balun bandpass filter for wide stopband attenuation base on stepped impedance resonators," in *Proc. Asia–Pacific Microw. Conf. (APMC)*, Kyoto, Japan, Nov. 2018, pp. 1220–1222.

[13] C.-Y. Huang, G.-Y. Lin, and C.-W. Tang, "Design of the wide-stopband balun with stepped coupled lines," in *Proc. Asia–Pacific Microw. Conf. (APMC)*, Kyoto, Japan, Nov. 2018, pp. 1103–1105.

[14] Y.-W. Lin, J.-C. Lu, and C.-Y. Chang, "Design of high-order wideband planar balun filter in *S*-plane bandpass prototype," *IEEE Trans. Microw. Theory Techn.*, vol. 60, no. 7, pp. 2124–2130, Jul. 2012.

[15] D. Tang, C. Han, Z. Deng, H. Jenny Qian, and X. Luo, "Substrate-integrated defected ground structure for single- and dual-band bandpass filters with wide stopband and low radiation loss," *IEEE Trans. Microw. Theory Techn.*, vol. 69, no. 1, pp. 659–670, Jan. 2021.

[16] C. Han, D. Tang, Z. Deng, H. J. Qian, and X. Luo, "Filtering power divider with ultrawide stopband and wideband low radiation loss using substrate integrated defected ground structure," *IEEE Microw. Wireless Compon. Lett.*, vol. 31, no. 1, pp. 113–115, Feb. 2021.

[17] R. Garg, I. Bahl, and M. Bozzi, *Microstrip Lines and Slotlines*, 3rd ed. Norwood, MA, USA: Artech House, 2013.

[18] D. M. Pozar, *Microwave Engineering*, 4th ed. New York, NY, USA: Wiley, 2012.

[19] C.-L. Hsu and J.-T. Kuo, "A two-stage SIR bandpass filter with an ultra-wide upper rejection band," *IEEE Microw. Wireless Compon. Lett.*, vol. 17, no. 1, pp. 34–36, Jan. 2007.

[20] K. S. Ang, Y. C. Leong, and C. H. Lee, "Analysis and design of miniaturized lumped-distributed impedance-transforming baluns," *IEEE Trans. Microw. Theory Techn.*, vol. 51, no. 3, pp. 1009–1017, Mar. 2003.

[21] L. Kun Yeung and K.-L. Wu, "An LTCC balanced-to-unbalanced extracted-pole bandpass filter with complex load," *IEEE Trans. Microw. Theory Techn.*, vol. 54, no. 4, pp. 1512–1518, Jun. 2006.

[22] J.-S. Hong, *Microstrip Filters for RF/Microwave Applications*, 2nd ed. New York, NY, USA: Wiley, 2011.

[23] S.-C. Lin, P.-H. Deng, Y.-S. Lin, C.-H. Wang, and C. H. Chen, "Wide-stopband microstrip bandpass filters using dissimilar quarter-wavelength stepped-impedance resonators," *IEEE Trans. Microw. Theory Techn.*, vol. 54, no. 3, pp. 1011–1018, Mar. 2006.

[24] C.-W. Tang and M.-G. Chen, "A microstrip ultra-wideband bandpass filter with cascaded broadband bandpass and bandstop filters," *IEEE Trans. Microw. Theory Techn.*, vol. 55, no. 11, pp. 2412–2418, Nov. 2007.